MDPI

Article

Antimony and Nickel Impurities in Blue and Green Copper Pigments

Sylwia Svorová Pawełkowicz [1,2,*], Barbara Wagner [1], Jakub Kotowski [3], Grażyna Zofia Żukowska [4], Bożena Gołębiowska [5], Rafał Siuda [3] and Petras Jokubauskas [3]

1   Biological and Chemical Research Centre, Faculty of Chemistry, University of Warsaw, 02-093 Warsaw, Poland; barbog@chem.uw.edu.pl
2   Institute of Inorganic Chemistry of the Czech Academy of Sciences, 250 68 Husinec-Řež, Czech Republic
3   Faculty of Geology, University of Warsaw, 02-089 Warsaw, Poland; j.kotowski@uw.edu.pl (J.K.); rsiuda@uw.edu.pl (R.S.); p.jokubauskas@uw.edu.pl (P.J.)
4   Faculty of Chemistry, Warsaw University of Technology, 00-664 Warsaw, Poland; zosia@ch.pw.edu.pl
5   Department of Mineralogy, Petrography and Geochemistry, AGH University of Science and Technology, 30-059 Cracow, Poland; goleb@agh.edu.pl
*   Correspondence: s.pawelkowicz@interia.pl

Abstract: Impurities in paint layers executed with green and blue copper pigments, although relatively common, have been studied only little to date. Yet, their proper identification is a powerful tool for classification of paintings, and, potentially, for future provenance studies. In this paper, we present analyses of copper pigments layers from wall paintings situated in the vicinity of copper ore deposits (the palace in Kielce, the palace in Ciechanowice, and the parish church in Chotków) located within the contemporary borders of Poland. We compare the results with the analyses of copper minerals from three deposits, two local, and one historically important for the supply of copper in Europe, i.e., Miedzianka in the Holy Cross Mountains, Miedzianka in the Sudetes, and, as a reference, Špania Dolina in the Slovakian Low Tatra. Optical (OM) and electron microscopy (SEM-EDS), Raman spectroscopy, and laser ablation inductively coupled plasma mass spectrometry (LA-ICP-MS) have been used for a detailed investigation of the minute grains. Special attention has been devoted to antimony and nickel phases, as more unusual than the commonly described iron oxides. Analyses of minerals from the deposits helped to interpret the results obtained from the paint samples. For the first time, quantitative analyses of copper pigments' impurities have been described.

Keywords: copper pigments (azurite; malachite); impurities/admixtures; antimony; nickel; provenance studies

1. Introduction

Copper minerals have been used as pigments in paintings almost since the beginning of art, though they were not as widespread as earth pigments [1]. Scott dates the first use of azurite to the 6th millennium BC [2,3]. Azurite ($2CuCO_3 \cdot Cu(OH)_2$) [1,2] and malachite ($CuCO_3 \cdot Cu(OH)_2$) [1,2] are cited as the most common copper-based minerals, but others have also been identified in painted works of art: copper sulphates (antlerite—$Cu_3(SO_4)(OH)_4$ [4–6]; brochantite—$Cu_4(SO_4)(OH)_6$ [5–9]; posnjakite—$Cu_4SO_4(OH)_6 \cdot H_2O$ [10–12]; dolerophanite—$Cu_2O(SO_4)$ [13]), copper and mixed-cation chlorides (copper trihydroxychloride isomers with the formula $Cu_2Cl(OH)_3$—atacamite [3,5,11,12]; paratacamite [4,12,14]; clinoatacamite [2]; botallackite [2]; calumetite—$CaCu_4(OH)_8Cl_2 \cdot 3.5H_2O$ [2,11]; zincian paratacamite—$Cu_3(Cu,Zn)Cl_2(OH)_6$; and herbertsmithite—$Cu_3Zn(OH)_6Cl_2$ [15,16]; or cumengeite—$Pb_{21}Cu_{20}Cl_{42}(OH)_{40} \cdot 6H_2O$ [12,16]), copper and mixed-cation phosphates (pseudomalachite—$Cu_5(PO_4)_2(OH)_4$ [12,17]; veszelyite—$(Cu,Zn)_2Zn(PO_4)(OH)_3 \cdot 2H_2O$ [17]), copper and mixed-cation arsenates (conichalcite—$CaCu(AsO_4)(OH)$ [4,13,14]; olivenite—$Cu_2(AsO_4)(OH)$ [18]; adamite—$Zn_2(AsO_4)(OH)$ [18]; mixite—$BiCu_6(OH)_6$

$(AsO_4)_3(H_2O)_3$ [19,20]), mixed-cation copper carbonates (aurichalcite—$(Cu, Zn)_5(CO_3)_2(OH)_6$ [21]; rosasite—$CuZn(CO_3)(OH)_2$ [22,23]), copper silicates (chrysocolla—$(Cu, Al)_2H_2(Si_2O_5)$ $(OH)_4 \cdot n(H_2O)$ [3,24,25]), copper oxides (cuprite—Cu_2O [15]; tenorite—CuO [26,27]), and copper organometallics (such as copper resinates, oleates proteinates, carbohydrates, and copper wax paints) [3,28].

If some of the above-mentioned pigments, such as copper chlorides (clinoatacamite [2], atacamite [12,29], paratacamite [12,14]), copper sulphates (brochantite [8,29], posnjakite [30]), and copper oxides (cuprite [15], tenorite [26,27]) were present in art objects, they were interpreted as alteration products of malachite or azurite; or evidence of use of a synthetic copper pigment [2,4,7,12], or natural admixtures [7,18,24,31] of malachite or azurite. Minerals like olivenite, adamite [18], and mixite [19] have been positively identified as natural impurities of copper carbonates. In some cases, it seems that the use of copper minerals other than carbonates was deliberate and helped to obtain the desired hue, like the use of copper sulphates reported by Spring [10] and Valadas et al. [32]. Additionally, natural admixtures of copper carbonates, such as the green-blue mixite reported by Berrie et al. [19], or the bluish posnjakite [24] had an influence on the final hue.

Chemical studies of paint layers executed with copper minerals revealed the presence of impurities. Although it is tempting to use them to determine the provenance of the pigments, it still seems that the state of the art is insufficient to draw far-reaching conclusions. Most studies report common impurities of copper minerals [33]. Until now, only few articles on painting materials addressed more unusual admixtures which could potentially be regarded as specific markers of the provenance of a copper pigment, or could simply bring new insights into old masters' painting techniques and their preferences in pigment selection [12,13,20,34–36].

In this paper, we present the results of analyses of copper pigments' impurities identified in paint samples obtained from three wall paintings situated in three different regions of Poland that are rich in copper minerals: the upper dining room polychromy in the former Cracow Bishops' Palace in Kielce near the Miedzianka deposit in the Holy Cross Mountains (the HCM) dated to the end of the 17th c; the painted decoration of the piano nobile in the Ciechanowice Palace near Miedzianka in the Rudawy Janowickie—the Sudetes, dated to the second half of the 16th c with subsequent repaintings, and the polychromy of the Chotków church vault in lubuskie voivodeship close to the Legnica-Głogów copper district, dated to the 14th c. Two of these localities were known at the time when the artworks were created (the HCM [37], and the Sudetes [38]), while the Legnica-Głogów copper ore deposit is reported to be discovered in the 20th century, due to the considerable depth of the deposit.

Although all three localities are situated within the contemporary borders of Poland, in the past, Ciechanowice, as part of Silesia, was constantly shifting from Polish to Bohemian and Prussian rule, while Chotków was part of the Brandenburg state. Only Kielce was part of the so-called Old Polish Industrial Region. Due to mining problems and scarcity of the ores, the deposits in the HCM and the Sudetes were rather of local significance. Their development was linked with the interruption of trade in Hungarian copper after the Turkish invasion. Archival studies confirmed that azurite and malachite from Miedzianka in the HCM were sold to painters from Cracow and used inter alia in the Wawel Castle decorations; moreover, there is a high likelihood that they were exported to Bruges and Leipzig [39]. The main sources of copper pigments were Sinai (in ancient times), Hungary (in the Middle Ages), and Germany (in modern times; Saxony, Tyrol, Saarland) [40].

Although we refer to common impurities, such as iron oxides and barite, in the paper, particular attention has been devoted to antimony and, to a lesser extent, nickel compounds, as they had never been studied before in the context of pigment identification. Antimony and nickel impurities were also studied in copper mineral specimens from the deposits in the HCM and the Sudetes, and Špania Dolina (formerly Hungary) as a comparative reference.

The three deposits (Miedzianka in the HCM, Miedzianka in the Sudetes, and Špania Dolina) differ considerably from the geological point of view. In the HCM Miedzianka, primary calcite veins bearing hydrothermal ore mineralization occur within the Devonian limestones exclusively [41]. The calcite veins bear sulfides and sulfosalts. The main ore minerals are tennantite-(Zn) and chalcopyrite [42]. Copper ions mobilized during the weathering of the primary sulfide mineralization were carried away from the limestones with ground waters and were absorbed at the contact between the Devonian limestones and the Triassic sediments. There, so-called contact ores were formed, comprising Triassic clays and sandstones impregnated by copper carbonates [43]. The most common representative of the secondary copper minerals is malachite [37]. It usually forms earthy cryptocrystalline aggregates weighing up to several dozens of kgs. Malachite forms flowstone-like, dark green aggregates, too. This type of malachite may have been used for pigment production. Azurite usually forms earthy or compact masses. Aggregates of this mineral can be up to several cms in size. Automorphic azurite crystals up to 1 cm in size are much rarer.

The polymetallic ore deposit in Miedzianka in the Sudetes is situated in the eastern part of the metamorphic envelope of the Karkonosze granitoid massif [44]. Ore mineralization mainly occurs in amphibolites, amphibolite, or quartz-sericite schists. The main ore minerals include: chalcopyrite, bornite, chalcocite, and minerals from the tetrahedrite group [45]. There are many secondary copper minerals in the weathering zone of the Miedzianka deposit, mainly arsenates and phosphates [46]. Malachite and azurite are rare. Malachite forms thin crusts on the surfaces of rocks containing weathered copper sulfides.

The Špania Dolina deposit is situated in the Starohorské Mountains (central Slovakia). Primary copper mineralization occurs in quartz–siderite–sulfide veinlets and as impregnations. Mineralized zones are present in the Permian sandstones and conglomerates [47]. The main copper ore mineral is the variety of tetrahedrite. This mineral is accompanied by chalcopyrite and variable amounts of other ore minerals [48]. There are many secondary minerals in the oxidation zone—mainly copper arsenates and sulfates [49]. The weathering zone of the Špania Dolina deposit is famous for large accumulations of copper carbonates. Malachite occurs as globular and reniform aggregates, up to several cms in diameter. This type of malachite was used to produce a high-quality green pigment. Azurite forms tiny crystals that form crusts on rock surfaces. Sometimes one may come across larger, cryptocrystalline azurite aggregates, with a diameter of up to several cms. Noteworthy is the high activity of antimony in the weathering zone of the Špania Dolina deposit [49]. This element is released during weathering of the tetrahedrite series and can form its own secondary minerals. It can also be incorporated into the crystal lattices of other minerals.

Analysis of trace minerals present in paint samples is a challenging task, mainly due to the small amounts of material (limited number of samples, small samples, thin paint layers, only few grains of impurities present, particularly minute grains of impurities—in this case, the grains ranged from 1 to 7 µm). Heterogenous composition of paint layers (mixed organic and inorganic components, variable elemental composition, variable size of the measured grains) is another complication that needs to be overcome, and is frequently mentioned by researchers [36]. Moreover, as the objects of art were exposed to adverse environmental conditions over a prolonged period, they were affected by degradation processes. Especially pigments in wall paintings are exposed to considerable humidity variations, as well as salts and microorganisms; together, these lead to alterations of minerals [12,50]. Hence, identification of the mineral present in the paint layer may be difficult, and identification of the primary mineral used by the artist is even more complicated. All of the studied samples were collected from wall decorations, and some of them suffered visible color alterations.

Unfortunately, minute size of the impurities made it impossible to examine them through an optical microscope, thus making it impossible to draw conclusions about their color and influence on the final hue of the paint layer. Based on energy dispersive spectrometry, their elemental composition was determined quantitively, but due to the limited space resolution of Raman spectroscopy coupled with optical microscopy, the

molecular structure still needs to be addressed. Nevertheless, we consider presenting reliable data on elemental composition of trace elements and their compounds present in copper-rich paint layers as a valuable contribution to technical art history.

2. Materials and Methods

Micro-samples of green and blue paint layers and samples of minerals for stratigraphic studies were embedded in epoxy resin, Epofix (Struers), and polished on a mechanical grinder-polisher Labo-Pol 2 (Struers ApS, Ballerup, Denmark) using silicon carbide waterproof abrasive foils at successive grits of 180, 320, 500, 1000, 2000, and 4000. For the final diamond polishing, suspensions of 3 and 1 μm were used.

Cross-sections were further studied in visible light using an Olympus CX41 microscope with an Olympus UC30 camera (Olympus Corporation, Tokyo, Japan).

Elemental composition measurements and initial mineral identification were performed using a Jeol scanning electron microscope (SEM) JSM-6510LV (JEOL Ltd., Tokyo, Japan) equipped with an energy dispersive spectrometer (EDS) by Oxford Instruments (Abingdon, UK), with a silicon drift detector (X-act, Oxford Instruments, Abingdon, UK). The first EDS semi-quantitative measurements were carried out with no standardization in low vacuum mode under the pressure of 50 Pa and accelerating voltage of 20 kV, working distance of 10 mm, and acquisition time from 35 to 100 s.

After this preliminary analysis, samples of paint layers with more unusual impurities were selected for further studies, including molecular identification of the main copper pigment, and of bigger grains of impurities in the layers, by means of Raman spectroscopy. μRaman measurements were performed with a Nicolet Almega Dispersive Raman Spectrometer (XR, Thermo Fisher Scientific, Waltham, MA, USA), equipped with an Olympus confocal microscope and motorized stage. Depending on the properties of the sample, a 780 or 532 nm excitation line was used. Power of the laser was reduced to 25–50% to avoid sample overheating. Typical exposure time was 15–45 s. Each spectrum was collected from two scans. Spectral resolution was approximately 2 cm^{-1}.

Small grains of impurities in copper-based paint layers were subsequently analyzed with a ZEISS SIGMA VP field emission scanning electron microscope (Carl Zeiss Microscopy GmbH, Oberkochen, Germany) equipped with two energy-dispersive X-ray spectrometers Bruker XFlash 6|10 (SEM-EDS) (Bruker, Karlsruhe, Germany). The analyses were conducted under a 10 kV accelerating voltage, 0.77 nA beam current, and 7.7 mm working distance. The counting times applied were 300 s for elemental mappings, and 60 s for point analyses. The most interesting impurities were mapped. Samples were then repolished and carbon-coated, with coating thickness of 20 nm, to ensure good electrical conductivity. EDS was recalculated to chemical composition using NIST DTSA-II public domain software by the National Institute of Standards and Technology (NIST). For standard-based quantification of the analyzed material, sets of metal (SPI 44 metals) and mineral standards (SP088—Cameca geological set) were used. NIST DTSA-II allows two kind of standards, for composition, and for peak-reference. Metal standards for elements were used as composition standard only if no mineral standard for a given element was in the set, otherwise, it was used only as peak-shape standard. Composition standards were as follows: Ca-diopside, Ni from metal Ni, Cu from metal Cu, As from $ZnAs_2$, Si from albite, Pb from PbTe, In from metal In, Sb from metal Sb, Sn from SnO, P from apatite. For the K52 sample, we present semi-quantitative data without normalization to 100%, from Bruker-Esprit software; the results are expressed as oxides wt%. This sample contains Br, and the available standard of Br–Tl(Br,I) is not stable under the electron beam and might contaminate the vacuum chamber.

Samples of minerals were further analyzed with Laser Ablation Inductively Coupled Mass Spectrometry (LA-ICP-MS) to detect trace elements. An NexION 300D Inductively Coupled Plasma Mass Spectrometer (PerkinElmer, Waltham, MA, USA) equipped with LSX-213 laser ablation system (CETAC, Omaha, NE, USA) was used during the measurements, with Argon (Ar) as carrier gas. Three ablation lines were selected on the surface of the

sample (E = 5.0 mJ; φ = 100 μm; SR = 50 μm/s; 20Hz). Transient signals were recorded and evaluated for subsequent elemental quantification for the selected isotopes ([23]S, [35]Cl, [39]K, [43]Ca, [45]Sc, [49]Ti, [51]V, [53]Cr, [55]Mn, [57]Fe, [59]Co, [61]Ni, [65]Cu, [66]Zn, [71]Ga, [75]As, [85]Rb, [88]Sr, [89]Y, [90]Zr, [93]Nb, [95]Mo, [106]Pd, [107]Ag, [111]Cd, [113]In, [118]Sn, [121]Sb, [133]Cs, [137]Ba, [139]La, [140]Ce, [141]Pr, [146]Nd, [147]Sm, [153]Eu, [157]Gd, [159]Tb, [163]Dy, [165]Ho, [166]Er, [169]Tm, [172]Yb, [175]Lu, [178]Hf, [182]W, [193]Ir, [195]Pt, [197]Au, [208]Pb, [209]Bi, [232]Th, [238]U). The LA-ICP-MS signals were background-corrected and integrated using Microsoft Excel. Standard glass NIST SRM 610 was used as the external standard. A rough estimation of elemental samples inhomogeneity was approximated by 2D map reconstruction based on 3-line ablation.

The unpolarized μRaman spectra of minerals were collected in back-scattered geometry with a Horiba Labram HR (Horiba, Ltd., Kyoto, Japan) spectrometer integrated with an Olympus BX 40 confocal microscope. The parameters of Raman measurements were as follows: estimated analytical spot size of ~1–2 μm, 532 nm line of a solid-state Nd-YAG laser (10 mW), 1800 g/mm grating, microscope objective 100×, acquisition time of 20, and accumulation of 2 scans. The spectra were recorded in the range of 4000–50 cm^{-1} on a randomly oriented surface of crystals mounted in epoxy resin in 0.7-inch plate that was used also for SEM-EDS studies.

3. Results

3.1. Copper Pigments Paint Layers

During the first stage, samples of paint cross-sections were studied with optical and electron microscopy. Based on the qualitative and semi-quantitative elemental composition obtained by SEM-EDS, further analyses were planned to identify the molecular structure of the main components and impurities. In the second stage, X-ray intensity maps were collected from the small antimony and nickel-rich grains, to establish elemental distribution within the grains. Finally, quantitative EDS measurements of the grains were performed, and the results are summarized in Tables 1 and 2.

3.1.1. Identification of the Main Components and Common Impurities of Paint Layers

- Upper dining room in the former Cracow Bishops' Palace in Kielce, near the Miedzianka copper deposit in the HCM.

Contrary to initial expectations, only one sample with azurite was identified in the room. In sample K52 (Figure 1), azurite (399/400, 1093 cm^{-1}) with individual grains of malachite (270, 431 cm^{-1}), hematite (~292, 224 cm^{-1}), and calcite (1086 cm^{-1}) were detected by means of Raman spectroscopy. In all the other blue areas, smalt was present in the layer dated to the first decoration, ca 1640. In the subsequent overpaints, a mixture of lead white, charcoal black, Prussian blue, and artificial ultramarine were identified by EDS, μRaman spectroscopy, and optical microscopy. Copper pigments were detected in the green areas; in most of the samples, malachite (178, 217, 268, 431, 534, 1058, 1098 cm^{-1}) with, probably, cuprite (150, 210 cm^{-1}) and azurite (398, 1094 cm^{-1}) as impurities. Copper sulphates–posnjakite (444, 505, 974 cm^{-1}) were detected, mixed with malachite (177, 269, 431 cm^{-1}) and impurities of hematite (220, 291, 406 cm^{-1}). Thus, posnjakite should rather be interpreted as an alteration product of malachite, and not the initially used mineral [12,30].
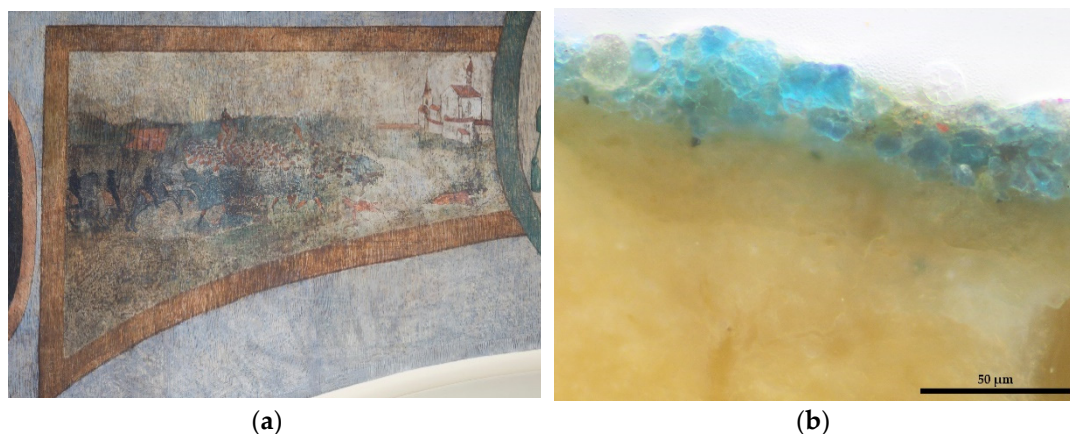
Figure 1. (**a**) Photo of the area where sample K52 was collected, photo by K. Opiłło; (**b**) cross-section of sample K52 with an azurite layer, magnification ×400.

- Piano nobile of the Ciechanowice Palace (before 1945, Rudelstadt) near the polymetallic deposit in the Rudawy Janowickie (the Sudetes).

  The 16th century decoration of the piano nobile is rich in copper pigments. In the green areas of the oldest painted decoration, malachite with typical impurities of iron oxides was detected. High amounts of silica were found during EDS analyses; some clusters of silica and copper minerals were detected as well. In the blue areas, azurite (153, 170, 248, 399, 1094 cm^{-1}) with impurities of rutile (447, 607 cm^{-1}), goethite (246, 300, 388, 500 cm^{-1}), and calcite (1086 cm^{-1}) were identified. Azurite paint layers were particularly rich in titanium and iron oxides with manganese and phosphorous impurities. Less common grains of barium sulphate were also found. In one case, EDS measurements revealed zinc arsenate or copper-zinc arsenate. In samples G5 and G4 (Figure 2), collected from the blue-green areas of a layer belonging to a later decoration, Raman spectroscopy measurements did not identify the copper component detected with EDS—probably due to pigment degradation [51]; only calcite (1085 cm^{-1}) was detectable.

Figure 2. (**a**) Photo of the area where samples G4 and G5 were collected; (**b**) cross-section of sample G4 with a bluish-green copper pigment layer on top of the sample, magnification ×200.

- Floral decoration of the vaults in the Chotków church (before 1945, Hertwigswaldau), near the Legnica-Głogów copper deposit.

  Malachite (179, 215, 268, 432, 1101 cm^{-1}) and tenorite (294, 603 cm^{-1}) were identified in the green and black leaves of the vegetal decoration of the church's vaults. In this case, tenorite is an alteration product of malachite, resulting from the action of oxalic acid as metabolic product of microorganisms, or the influence of alkaline environment on finely

ground malachite grains [27,50,52,53], because, most probably, the painting was executed in fresco technique. This degradation is clearly visible in the samples where the green layer meets the black layer (see Figure 3b). Chemical analyses of samples Ch 33 and Ch 35 detected calcium oxalate–weddellite (1475, 909 cm^{-1}), which would support the biodegradation hypothesis. Influence of high temperatures is also reported to be the cause of degradation of azurite to tenorite [26], but no evidence of fire in the church was found, so this cause may be ruled out. Calcite (1131, 1085, 492 cm^{-1}) and gypsum (1007 cm^{-1}) were also detected in the copper pigments layer.

(**a**) (**b**)
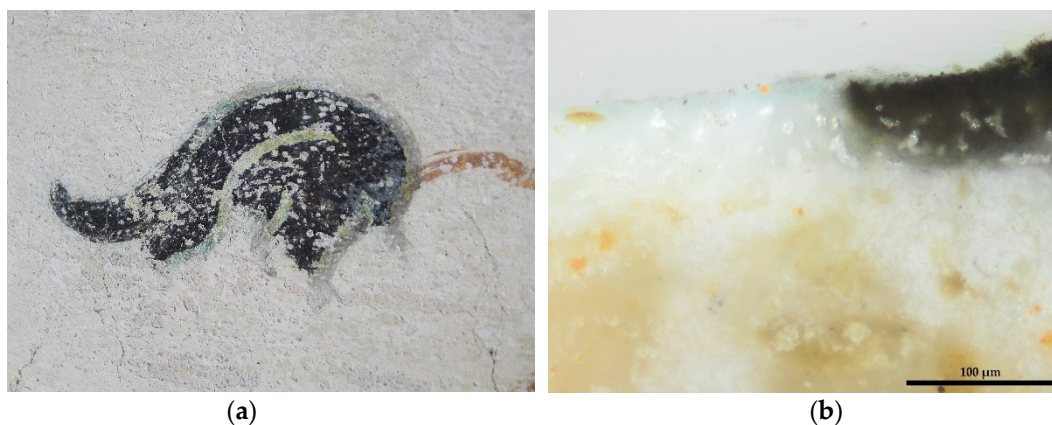
Figure 3. (**a**) Photo of the area where sample Ch35 was collected; (**b**) cross-section of sample Ch35 with a malachite layer, and tenorite as alteration product, magnification ×200.

3.1.2. Antimony and Nickel Impurities Analysis

For the second phase of the research, samples containing unusual antimony and nickel impurities were selected. By means of electron microscopy, X-ray intensity mapping of individual grains and semi-quantitative (sample K52) and quantitative (samples G4, Ch33, Ch35) elemental point measurements were performed (see Tables 1 and 2).
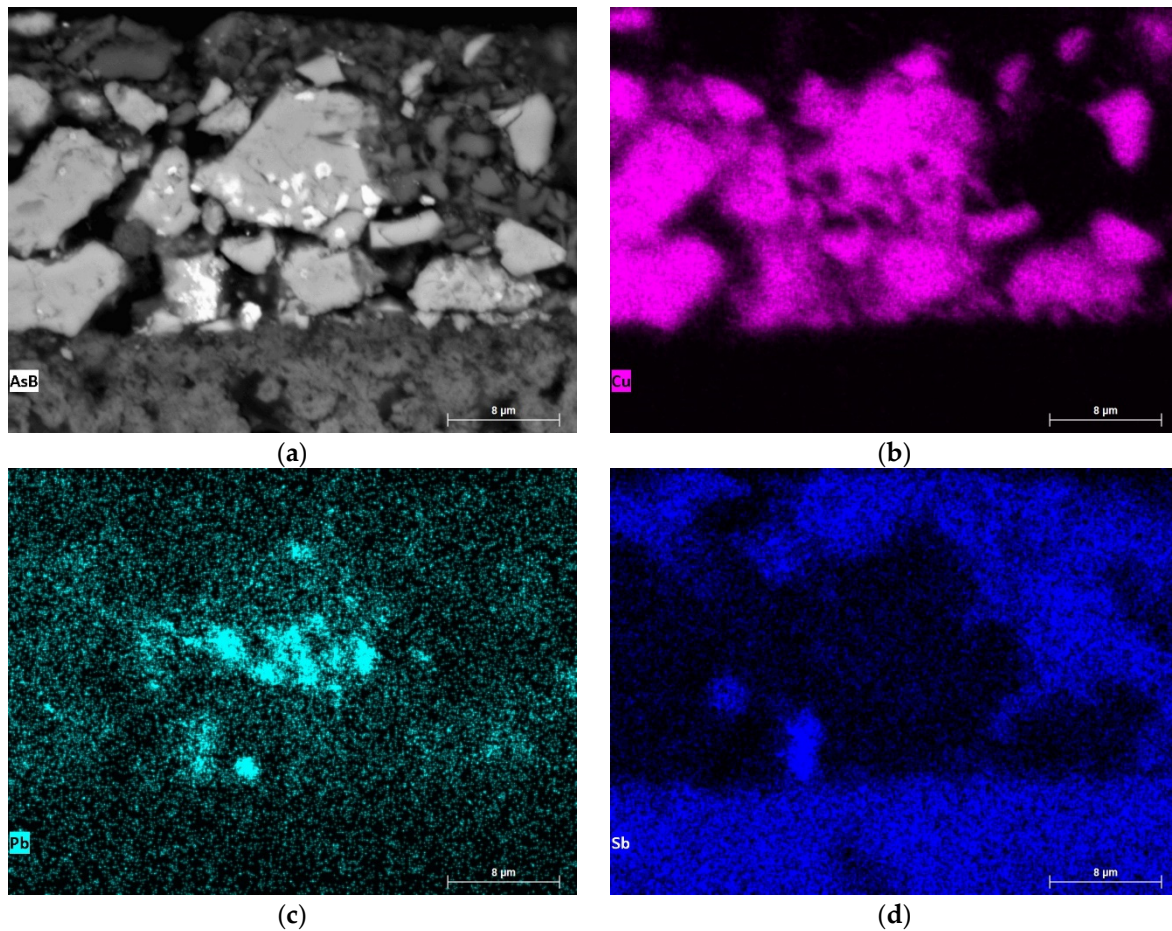
Table 1. Semi-quantitative elemental analysis of selected Sb-bearing grains in azurite paint layer (sample K52) by EDS, expressed in wt% oxygen by stoichiometry.

No	Br$_2$O	Al$_2$O$_3$	SiO$_2$	K$_2$O	FeO	CuO	As$_2$O$_5$	Sb$_2$O$_3$	PbO	P$_2$O$_5$	CaO
K52/6	4.4	9.0	6.3	0.4	6.0	4.4	20.0	2.6	25.9	0.6	0.4
K52/7	2.3	8.2	4.3	0.4	6.5	6.7	17.3	3.0	20.6	0.0	0.5

- Sample K52 from the former Cracow Bishops' Palace in Kielce.

EDS measurements revealed the presence of areas of lead concentration in azurite crystals—probably inclusions of cerussite, Pb(CO$_3$), a mineral associated with azurite in copper deposits [54]. In some cases, the lead-rich areas also contained antimony (Figure 4). Along with relatively small amounts of antimony (~3 wt% Sb$_2$O$_3$), elevated concentrations of lead (~20–25 wt% PbO), arsenic (~20 wt% As$_2$O$_5$), and bromine (~2–4 wt% Br$_2$O) were detected. Other elements detected in the antimony-bearing grains were silicon, potassium, and, probably, phosphorus. The elemental composition may be indicative of a mixture. A possible mineral could be murdochite PbCu$_6$O$_{8-x}$(Cl,Br)$_{2x}$—a common associate of malachite. Presence of cerussite, bindheimite (Pb$_2$Sb$_2$O$_6$O), and an arsenate is not ruled out. Mindat.org lists iron and phosphorous among common impurities of olivenite, a copper arsenate, while for bindheimite, it lists arsenic, bismuth, calcium, iron, and sodium [54]. Moreover, bindheimite is an associate of azurite, malachite, and cerussite [54]. Substitution of Pb by Sb in bindheimite, as well as bindheimite hosting copper and arsenic has already been reported [55]. This mixture of minerals is, however, a vague hypothesis and would

need to be confirmed by supplementary studies. Presence of copper sulphosalts would be another possibility, yet no sulphur was found in the EDS analysis.

Figure 4. X-ray intensity maps of selected elements in the malachite layer of sample K52: (**a**) angle selective backscattered (AsB) electron image; (**b**) Cu map; (**c**) Pb map; (**d**) Sb map.

Table 2. Quantitative elemental analysis of selected Sb-bearing grains in green copper pigments layers (sample G4, Ch33, Ch35) by EDS expressed in wt% oxygen by stoichiometry.

No		Sb_2O_3	In_2O_3	P_2O_5	FeO	As_2O_5	CaO	PbO	SrO	NiO	Cl_2O_5	SnO	CuO	SiO_2
G4/1	wt%	0.04	0.15	0.05	0.00	0.40	1.78	47.48	0.24	0.09	0.76	17.52	8.64	0.48
	±	0.18	0.13	0.06	0.29	0.07	0.13	0.78	0.23	0.66	0.12	0.95	1.77	0.05
G4/2	wt%	1.09	0.08	0.00	0.24	0.08	0.59	0.13	0.00	1.08	0.27	92.78	1.99	0.63
	±	0.28	0.17	0.35	0.25	0.05	0.14	0.10	0.46	0.65	0.05	0.37	1.65	0.05
G4/4	wt%	22.66	0.37	0.22	0.00	2.01	0.63	8.69	0.00	23.46	0.17	2.52	39.55	1.66
	±	0.33	0.12	0.06	0.24	0.23	0.11	0.27	0.44	0.91	0.06	0.18	2.30	0.07
Ch33	wt%	34.36	0.00	0.00	0.00	0.67	1.94	44.43	0.00	1.56	0.28	0.00	4.78	1.67
	±	1.27	0.11	0.41	0.30	0.09	0.14	0.79	0.54	0.69	0.09	0.20	1.80	0.07
Ch35/1	wt%	25.83	0.06	0.11	0.05	0.18	0.93	0.39	0.08	26.52	0.01	3.04	45.15	0.73
	±	0.33	0.12	0.06	0.24	0.06	0.11	0.10	0.25	0.93	0.06	0.18	2.35	0.05
Ch35/2	wt%	4.07	0.00	0.00	0.12	12.31	7.61	49.73	0.25	0.18	1.35	0.29	0.00	2.43
	±	0.28	0.10	0.39	0.25	1.56	0.39	0.80	0.24	0.69	0.19	0.14	2.10	0.11
Ch35/4	wt%	0.19	0.11	0.10	0.00	0.54	6.81	4.02	0.00	46.27	2.95	0.00	21.63	10.13
	±	0.15	0.09	0.06	0.20	0.09	0.09	0.17	0.49	1.11	0.13	0.12	1.99	0.30
Ch35/5	wt%	29.71	0.16	0.00	0.00	1.79	3.55	45.98	0.00	0.88	1.26	0.06	6.35	3.27
	±	1.06	0.13	0.41	0.30	0.20	0.17	0.77	0.57	0.69	0.14	0.19	1.85	0.10

- Sample G4 from the Ciechanowice Palace.

In sample G4, EDS measurements revealed the presence of an antimony-rich grain (G4/4) with over 20 wt% Sb_2O_3 content, and grains (G4/1, G4/2) with antimony as trace element. The antimony-rich grain (G4/4) also contained a high percentage of nickel and copper. Moreover, some lead, tin, and arsenic were detected. The elemental composition may be indicative of an oxidized mineral zlatogorite ($CuNiSb_2$), or a mixture with breithauptite (NiSb), with lead and tin. Tin was the main component of one grain with antimony as trace element (G4/2); this could be cassiterite (SnO_2), and as for the other (G4/1) a lead-tin oxide [56] or a mixture of minerals containing lead, tin, and copper could be expected.

- Samples Ch33 and Ch35 from the church in Chotków.

In the samples from Chotków, minute antimony-bearing grains were quite numerous. All the measured particles contained, apart from often-elevated concentrations of antimony (two grains with the content of 25.83 and 29.71 wt% Sb_2O_3), different amounts of lead (ranging from 0.39 to 49.73 wt% PbO). In all measurements, nickel was detected, in variable amounts (0.18–46.27 wt% NiO). Again, as in the case of the Ciechanowice Palace, a Cu-Sb-Ni grain was detected (compare Ch35/1 and G4/4 in Table 2). Although most of the studied grains had irregular shapes, the grain measured as Ch35/1 (Figure 5) was characterized by angular, rod-like shape. In one measurement (Ch35/2), antimony was associated with lead and arsenic. Elemental composition of the grain in sample Ch33 and grain Ch35/5 is similar to bindheimite, with arsenic, copper, and silicon as trace elements. Grain Ch35/4 consisted mainly of nickel and copper, and lower amounts of silicon and calcium.
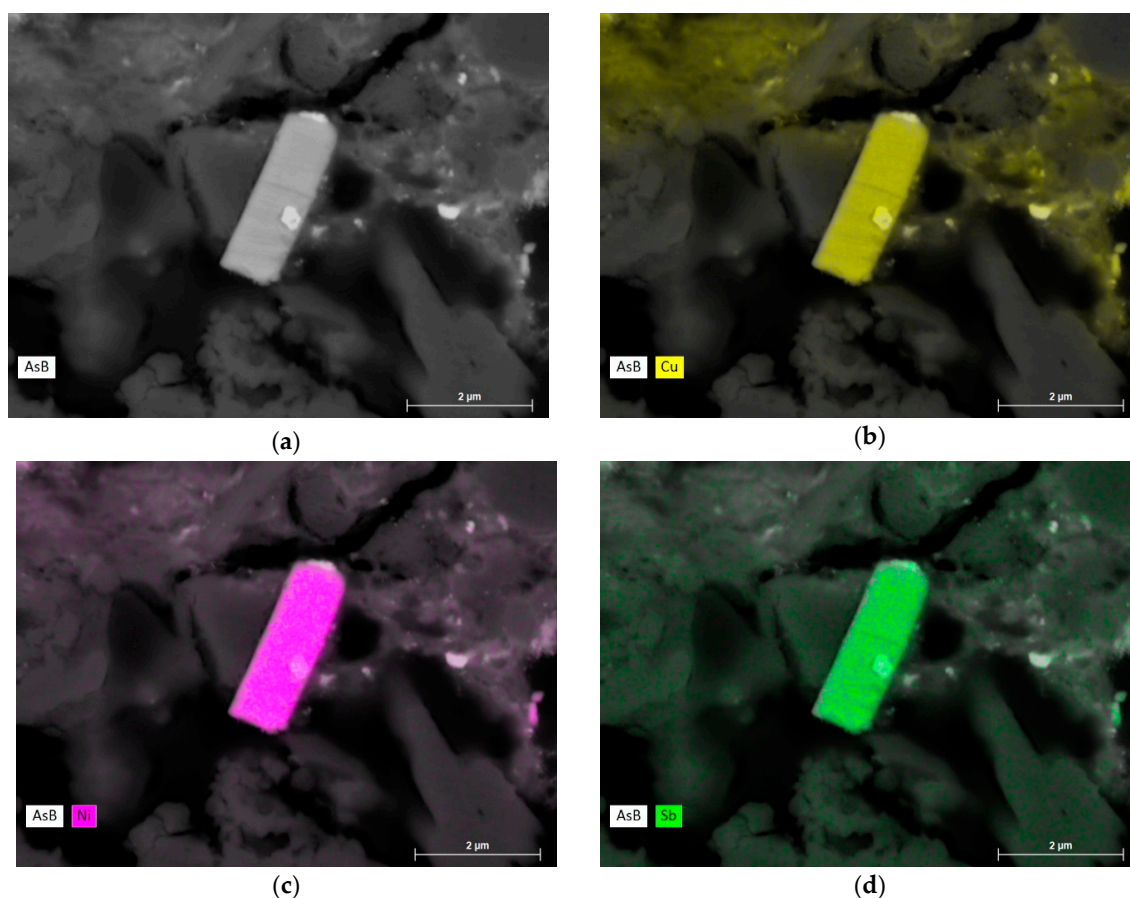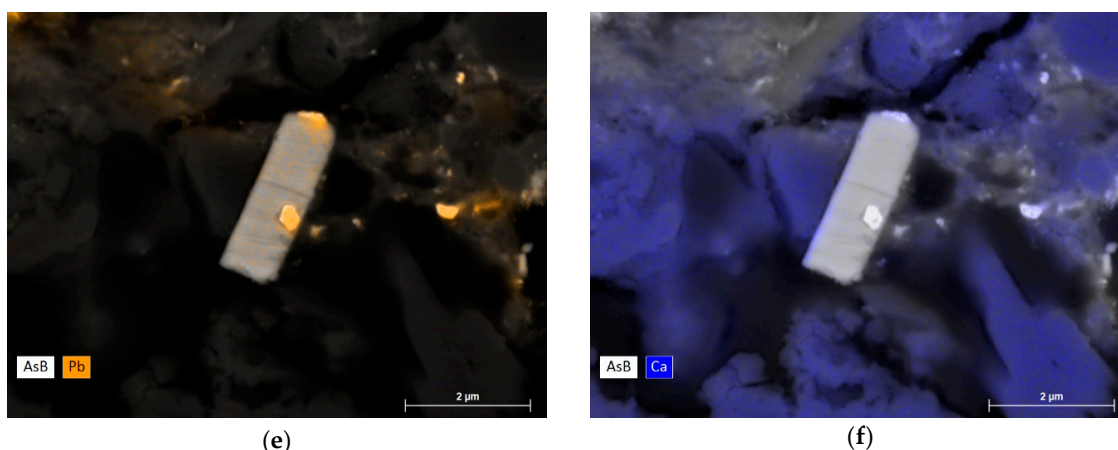

Figure 5. *Cont*.

(**e**)

(**f**)

Figure 5. (**a**) Angle selective backscattered electron image of the Cu-Ni–Sb particle in sample Ch35—quantitative measurement no. Ch35/1; (**b**–**f**) X-ray intensity maps of selected elements in malachite layer:(**b**) Cu map; (**c**) Ni map; (**d**) Sb map; (**e**) Pb map; (**f**) Ca map.

3.2. Trace Elements and Impurities in Minerals from Selected Copper Deposits

Concurrently with the examination of paint layers, samples of green and blue copper minerals from two possible local sources (Piotr mine shaft in Miedzianka in the HCM, and Segen Gotttes mine in Miedzianka in the Rudawy Janowickie Mts.—the Sudetes), and a third, more distant, but historically significant source, Piesky mine in Špania Dolina in the Slovakian Low Tatra (formerly Hungary), were examined. The mineralogical research was far from exhaustive but provided preliminary referential data for comparative analyses.

In the first step, samples of minerals were measured as fragments, without grinding, with EDS and LA-ICP-MS, and during the next step, cross-sections from the fragments were prepared, mapped, and measured with EDS. Finally, selected cross-sections, with significant concentrations of antimony detected with EDS were studied with point µRaman spectroscopy to characterize antimony-bearing phases. Unfortunately, due to the minute size of the particles, only the matrix in which they were embedded was identified.

Slovakian copper ore deposits, as well as Hungarian and Romanian, are reported to be dominated by Cu-Sb-As sulphosalts [57]. Therefore, we expected a high content of antimony and arsenic in the samples from Špania Dolina (samples 13–15, Table 4). However, preliminary studies showed inclusions of antimony in samples from Miedzianka in the Sudetes and Miedzianka in the HCM, but no antimony in the samples from Špania Dolina.

In the antimony-bearing grains of sample No. 3 (Miedzianka in the Sudetes), EDS measurements revealed, apart from antimony, high concentrations of arsenic, copper, iron, and small amounts of zinc, calcium, silicon, and aluminum (Figure 6). In the matrix, mainly copper was detected, with arsenic and zinc, suggesting a Cu-Zn arsenate with traces of lead, calcium, and silicon. In sample No. 9 (Miedzianka in the HCM), the predominant elements of the antimony-bearing grains were, again, arsenic, copper, lead, iron, while calcium, zinc, and silicon were detected in low concentrations. The matrix contained mainly copper with arsenic, and calcium, a small amount of zinc, and traces of lead and silicon, indicative of a Cu-Ca-Zn arsenate. In both cases, lead was in the structure of antimony-bearing grains. Nickel was found as trace element (≥1 wt%) in samples No. 5, 6, 7, and 11—all from the HCM deposit.
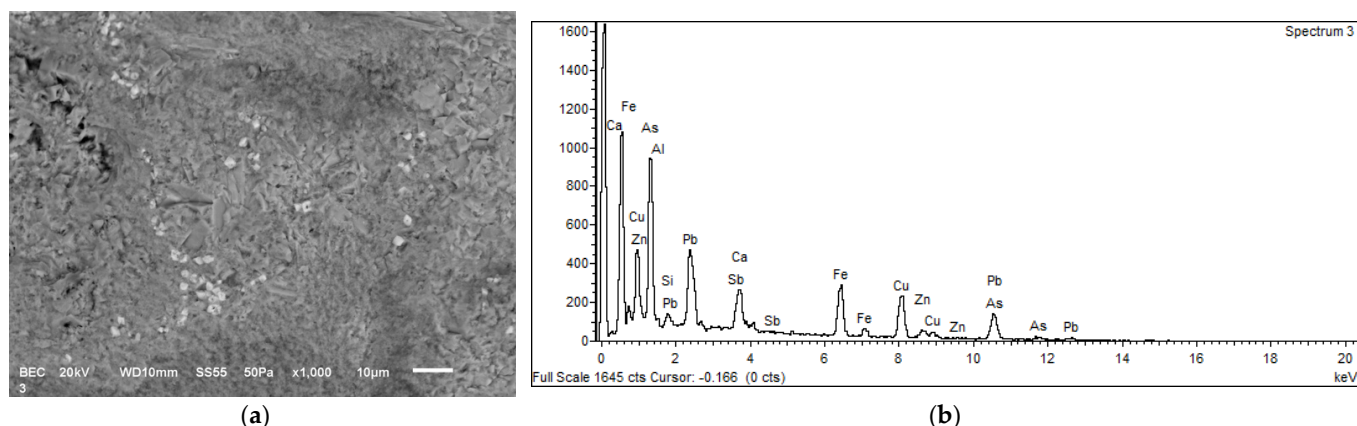
Figure 6. Sample 3. (**a**) backscattered electron image of the sample with minute Pb-Sb grains dispersed in the Cu-As matrix. (**b**) EDS spectrum of the grain.

Samples were measured with LA-ICP-MS, to examine the trace elements (Tables 3 and 4). The results were consistent with the EDS results; indeed, highest values of antimony content were observed in sample 3 (three areas of the sample were measured, and labeled as 3a and 3b (green area), 3n (blue area)), and 9. Yet in samples 5 and 10, some antimony concentrations were also recorded. Maps calculated based on LA-ICP-MS results showed considerable heterogeneity of the mineral samples (Figure 7). Thus, it is probably more representative to consider the maximal values than the mean. Antimony was usually, but not always, correlated with arsenic. The calculated correlation coefficient values of antimony were quite high for Sb-Pb (0.60–0.86) and Sb-As (0.68–0.82), but lower for Sb-Ni (0.37–0.45). Correlation coefficient of Sb-Cu could be high: up to 0.86 but could also be negative.

Table 3. Sb and Ni content in copper-based minerals coming from three different deposits, measured by LA-ICP-MS expressed in wt%, normalized to 100%.

|	Sample No	^{121}Sb			^{61}Ni		
		Mean	RSD, %	Max	Mean	RSD, %	Max
The Sudetes; Rudawy Janowickie Mts.; Segen Gottes mine	0	0.0027	24	0.0047	0.0001	441	0.0024
	1	0.0042	27	0.0081		n.d.	
	2a	0.0016	40	0.0042	0.0001	641	0.0063
	2b	0.0108	42	0.0267		n.d.	
	3a	1.8654	30	2.7633	0.0488	101	0.2907
	3b	1.0354	103	3.3960	0.0114	134	0.0734
	3n	1.1857	113	4.3240	0.0172	167	0.1625
The HCM; Miedzianka *	5	1.4889	40	3.3152	0.0442	126	0.2918
	6	0.0629	41	0.1911	0.8788	24	1.4702
	7	0.1021	31	0.2168	0.2240	22	0.3833
	8	0.0286	72	0.1476	0.0135	90	0.0696
	9	1.1879	30	1.9761	0.0396	109	0.2459
	10	0.1479	179	1.9714	0.1192	27	0.2209
	11	0.0495	118	0.2333	0.0002	554	0.0076
The Low Tatra; Špania Dolina; Piesky	13	0.1566	53	0.4745	0.0027	244	0.0490
	14	0.0542	86	0.3561	0.0021	216	0.0238
	15	0.2711	8	0.3552	0.0029	209	0.0353

* Samples 5–8 were collected from the Piotr shaft by Rafał Siuda; samples 9–11 were collected in the 1920s by Jan Czarnocki and are part of the collection of the Department of Natural History of the National Museum in Kielce.

Table 4. Calculated correlation coefficients in the mineral samples (3a, 3b, 9).

9	Ni	Cu	As	Sb	Pb	3a	Ni	Cu	As	Sb	Pb	3b	Ni	Cu	As	Sb	Pb
Ni	1.00	−0.14	0.75	0.45	−0.14	Ni	1.00	0.29	0.37	0.39	0.27	Ni	1.00	−0.29	0.40	0.37	0.22
Cu		1.00	−0.48	−0.80	−0.94	Cu		1.00	0.91	0.86	0.45	Cu		1.00	−0.62	−0.90	−0.93
As			1.00	0.70	0.20	As			1.00	0.82	0.42	As			1.00	0.68	0.44
Sb				1.00	0.60	Sb				1.00	0.60	Sb				1.00	0.86
Pb					1.00	Pb					1.00	Pb					1.00

−0.94   0.25   0.50   0.90   1.00
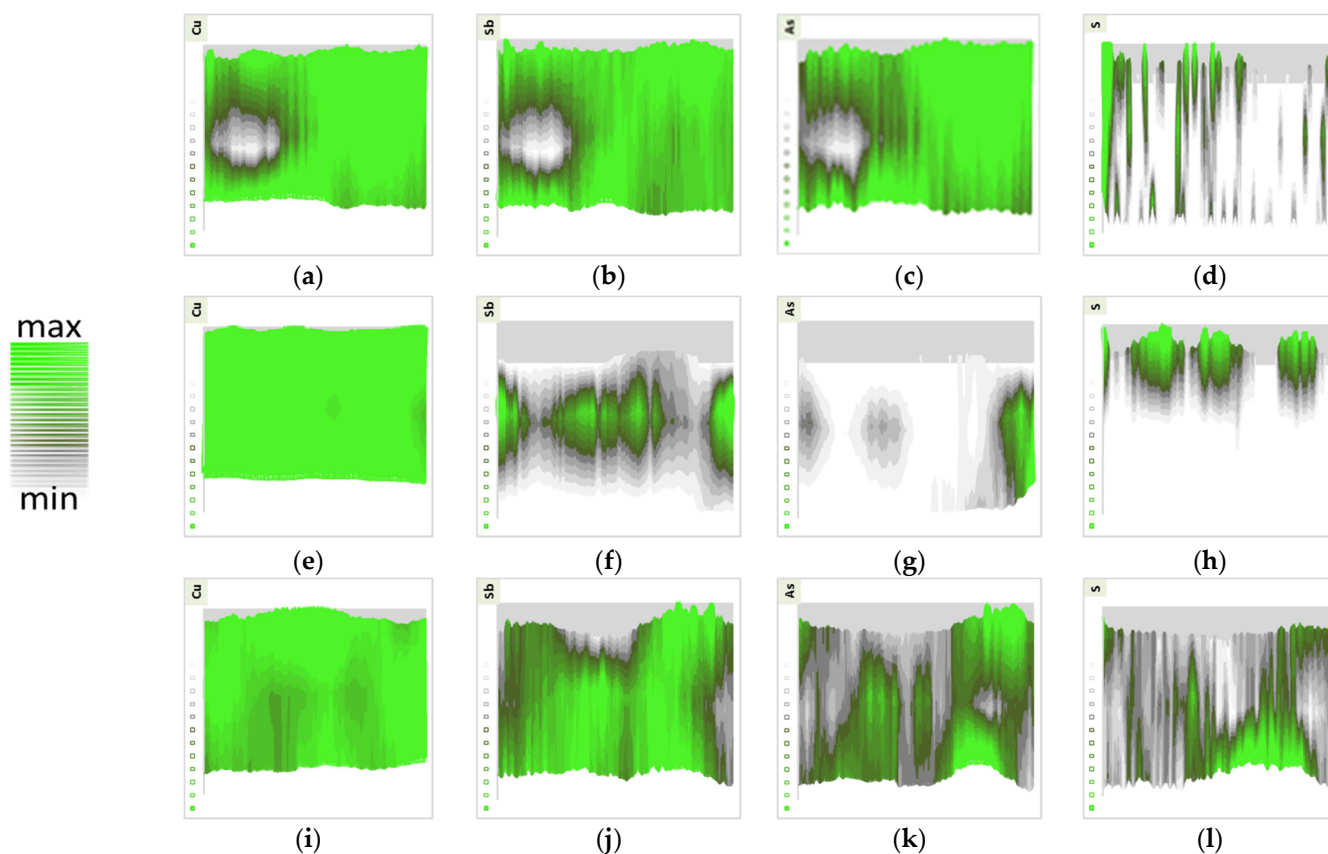
Figure 7. LA-ICP-MS maps showing the distribution of isotopes: Cu (**a**,**e**,**i**), and Sb (**b**,**f**,**j**), As (**c**,**g**,**k**), S (**d**,**h**,**l**) in samples 3a (**a–d**), 3b (**e–h**), 9 (**i–l**).

Samples 3 and 9 were measured with Raman spectroscopy in order to identify the matrix in which antimony-bearing crystals were present—the spectra are shown in Figures 8–10. Results obtained from the studied samples were compared with the data from the literature. Two Cu-arsenates—olivenite and conichalcite—were identified in both localities (Miedzianka in the Sudetes, and the HMC).

In the spectra (Figure 8), we observed one strong band at ~851-850 cm^{-1} attributed to AsO$_4$ symmetric stretching vibrations (v1), the bands at ~525 and 495 cm^{-1} related to AsO$_4$ symmetric bending vibrations (v4), and bands at 278 and 213 cm^{-1} attributed to Me-O stretching vibration [58]. The band of the hydroxyl-stretching region of olivenite is visible at 3479 cm^{-1} (Figure 9).

Figure 8 shows the spectra of olivenite and adamite from the RRUFF database (olivenite R050532, adamite R060593), two arsenates forming solid solutions. The maximum position of the bands can be indicative of substitutions in the chemical composition. The band at 3550 cm^{-1} is characteristic of pure adamite, and 3440 cm^{-1} of pure olivenite. In the studied case, it can be concluded that olivenite has a substitution of zinc, considering the shift of the bands towards lower wavelengths.
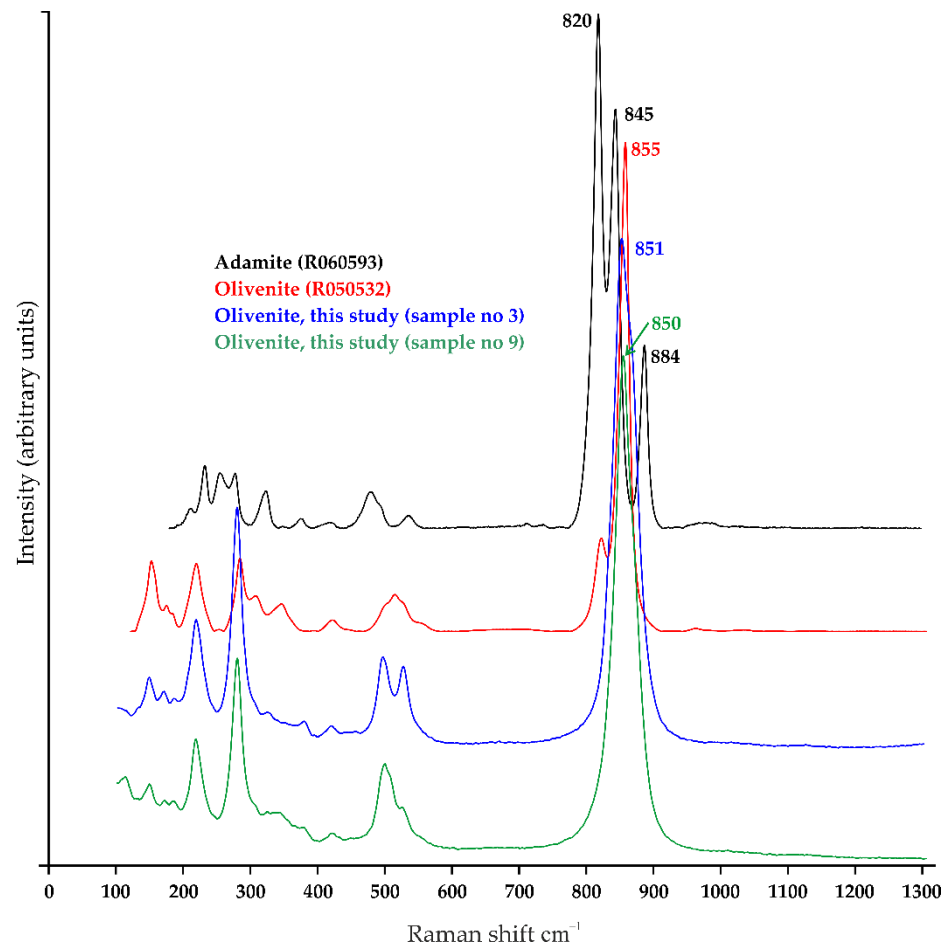
Figure 8. Reference spectra of olivenite and adamite, with the spectra measured in samples 3 and 9.
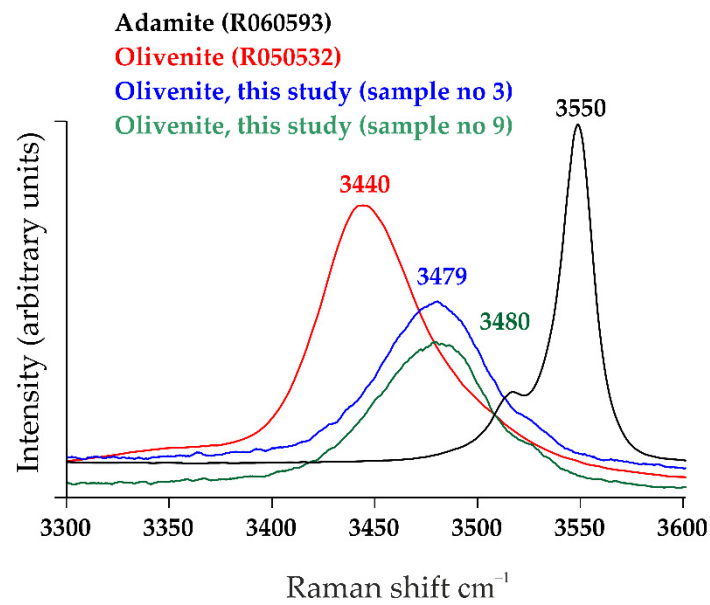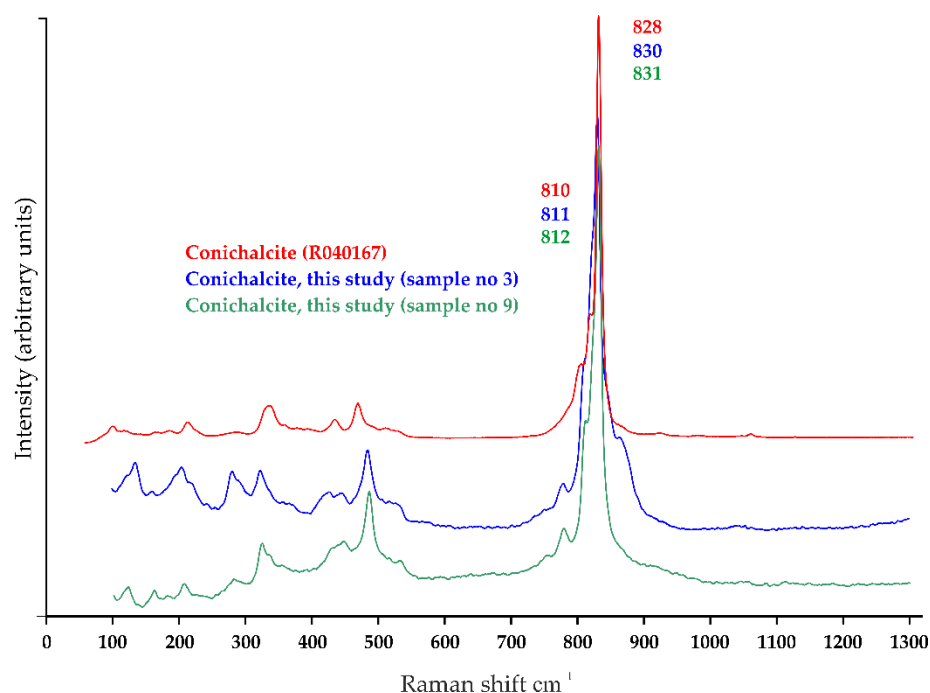

Figure 9. The band of the hydroxyl-stretching region in the reference spectra of olivenite and adamite, and the spectra measured in samples 3 and 9.

Figure 10. Reference spectra of conichalcite, with the spectra measured in samples 3 and 9.

Figure 10 shows spectra of conichalcite from the two localities. They were also compared with the standard spectrum of conichalcite (RRUFF R040167). The very strong band at 831 cm^{-1} and weak band at 812 cm^{-1} (v1) are related to the substitution of Zn for Cu in the structure of the studied minerals (solid solution conichalcite-austinite $(CaZn(AsO_4)(OH))$. Even a small admixture of the elements in the structure can contribute to the change of the position of the band maximum.

4. Discussion

In this paper, results of rare copper pigments impurities containing antimony and nickel were reported. Grains of Pb-Al-Br-As-Cu-Sb, Pb-Sn-Cu (with traces of Ni and Sb), Pb-Sb-Cu-Ni, Pb-As-Sb, Sn-Cu (with traces of Sb and Ni), Cu-Ni-Sb (with variable content of Pb and Sn), and Ni-Cu-Ca-Pb-Si were identified in paint layers containing copper pigments. In the mineral specimens, grains containing lead and antimony were found in the olivenite-adamite and conichalcite-austinite matrix in samples from Miedzianka in the HCM and the Sudetes.

The deposit in Miedzianka-Ciechanowice, Rudawy Janowickie (samples 0–3, Table 4), had already been studied by Siuda et al. [38]. Among the phases which, because of the presence of antimony, nickel, or accessory elements such as arsenic, could be helpful for the interpretation of results of paint layers analyses, annabergite $(Ni_3(AsO_4)_2 \cdot 8H_2O)$, minerals from tetrahedrite group, and arsenates, such as bayldonite $(PbCu_3(AsO_4)_2(OH)_2)$, cornwallite $(Cu_5(AsO_4)_2(OH_4))$, duftite $(PbCu(AsO_4)OH)$, clinoclase $(Cu_3AsO_4(OH)_3)$, olivenite (Cu_2AsO_4OH), scorodite $(Fe^{3+}AsO_4 \cdot 2H_2O)$, tyrolite $(CaCu_5(AsO_4)_2CO_3(OH)_4 \cdot 6H_2O)$, should be mentioned. Additionally, to the above listed minerals, olivenite-adamite and conichalcite-austinite were identified in the present study.

In the previous studies of Miedzianka deposit in the HCM (samples 5–11, Table 4), antimony was identified, along with sulphur, copper, and arsenic in the structure of miedziankite, a copper sulphosalt of the tetrahedrite and tennantite series solid solution [59]. Arsenic was identified also in arsenates (adamite, austinite, conichalcite, cornubite, olivenite, tyrolite, zincolivenite). Nickel was reported to be present in gersdorffite (NiAsS), and asbolane $((Ni,Co)_{2-x}Mn^{4+}(O,OH)_4 \, nH_2O)$ [54]. In the analysis of the soils of the former mining area, elevated concentrations of copper were strongly correlated with arsenic and nickel [60]. This is in accordance with our study, as nickel was detected as trace

element by EDS, and LA-ICP-MS results confirmed higher values of ^{61}Ni in the samples from Miedzianka in the HCM compered to Miedzianka in the Sudetes and Špania Dolina.

Mindat.org [54] mentions four valid minerals containing antimony in the Piesky mine in Špania Dolina (samples 13–15, Table 4): blue-green camerolaite ($Cu_6Al_3(OH)_{18}(H_2O)_2$ $[Sb(OH)_6](SO_4)$), blue-green cualstibite ($Cu_2Al(OH)_6[Sb^{5+}(OH)_6]$), steel to iron-gray variety of tetrahedrite ($Cu_6(Cu_4(Fe,Zn)_2)Sb_4S_{13}$), and yellow-brown tripuhyite ($Fe^{3+}Sb^{5+}O_4$). Bindheimite, although it is not present in the Piesky mine, was reported in numerous localities in Slovakia in the region of Banská Bystrica (Ľubietová, Staré Hory, Lomnistá, Jarčanisko), and Košice, Prešov, and Žilina [54]. In our study, we did not detect any antimony nor nickel impurities in the exceptionally pure malachite samples from Špania Dolina.

As shown above, antimony may be found in all three copper deposits, mostly in tetrahedrite series. Our study confirmed the presence of antimony-rich grains in both Miedzianka (in the Sudetes and the HMC). In the case of the samples from Špania Dolina, antimony traces were detected by LA-ICP-MS. Nickel-bearing minerals were reported in the literature in both Miedzianka (in the Sudetes and the HMC), while, according to mindat.org [54], no nickel phases were identified in the Piesky mine in Špania Dolina. Nevertheless, in a nearby copper deposit in Ľubietová several nickel-bearing species were confirmed (annabergite, asbolane, gersdorffite, nickelskutterudite, siegenite). Thus, the sole presence of antimony or nickel phases cannot be regarded as indicative of the pigment's origin. However, it might help exclude some possibilities, such as the Piesky mine, when elevated concentrations of nickel occurs. The high correlation coefficient between antimony and lead (see Table 4) in the studied minerals might be indicative of bindheimite, while the high correlation coefficient between antimony and arsenic suggests a tetrahedrite group.

The impurities of copper pigments most reported in the literature are red and brown iron oxides and hydroxides—hematite and goethite [12,33,34,61]. Identification of individual grains of malachite in azurite paint layers is also common [18,36,62,63]. Aru et al. [33] extended the list and divided the impurities identified in azurite specimens into two groups. As frequent, they classified goethite, malachite, hematite, and cuprite; and as less frequent—cerussite, cinnabar, quartz, calcite, rutile and anatase, rhodochrosite, carbon, beudantite, and jarosite. Barite was also reported as an admixture in azurite layers [36,63], or azurite transformed to atacamite mixed with paratacamite layers [12]. Raman spectroscopy confirmed barium carbonate in azurite [64]. The presence of zinc in azurite paint layers was reported by Delaney et al. [35] and Gabrieli et al. [20], suspecting smithsonite ($ZnCO_3$) admixture. Over the recent years, elemental X-ray fluorescence (XRF) imaging spectroscopy enabled detection of certain more specific elements (or correlated elements), such as antimony [34,65], arsenic [20,34], barium [34], bismuth [20,34], nickel [66], silver [34], zinc [20,35] in areas painted with copper pigments. In Table 5, we summarized the impurities reported in the literature.

Table 5. Impurities of copper-based paint layers reported in the literature.

Reference	Copper Mineral (Method)	Trace Elements (Method)	Impurity (Method *)	Data of the Art Object
Bordignon 2008 [64]	Azurite (SEM-EDS, µRaman)	Fe	Limonite, hematite, barite, Ba carbonate, atacamite, brochantite, dolomite, calcite, gypsum (SEM-EDS, µRaman)	Painted stone, Italy, not stated
	Malachite		Pseudomalachite	
Hradil 2008 [18]	Azurite (XRD)	As, Zn (pXRF)	Malachite, olivenite, adamite (XRD)	Panel painting, Slovakia, 15th c
Švarcová 2009 [12]	Azurite and malachite (XRD)	As, Ba, Zn, P (pXRF)	Malachite in azurite layer, atacamite, paratacamite posnjakite, barite, quartz (XRD); olivenite, adamite, pseudomalachite, iron oxides (SEM-EDS)	Wall paintings, Czechia, 14th c

Table 5. *Cont.*

Reference	Copper Mineral (Method)	Trace Elements (Method)	Impurity (Method *)	Data of the Art Object
Fabjan 2010 [65]	Copper green (pXRF)	As, **Sb**, Zn (pXRF)	-	Wall painting, Italy, 16th c
Buzgar 2014 [13]	Copper green	-	Conichalcite, malachite, Cu suphates (dolerophanite, brochantite) (μRaman)	Wall paintings, Romania, 16th c
Delaney 2014 [35]	Azurite (FORS)	Fe, Zn (Si, K, Ca, Ti, Mn, Pb) (pXRF, SEM-EDS)	-	Manuscript, Italy, 14th c
Salvadó 2014 [36]	Azurite	Ba, S (SEM-EDS)	Malachite (μSR-FTIR, μSR-XRD)	Panel paintings, Catalonia and Crown of Aragon, 15th c
Aceto 2017 [67]	Azurite (pXRF)	Bi (pXRF)	-	Manuscript, Italy, 14th c
Berrie 2016 [19]	Azurite (EBSD)	Bi not detected in pXRF	Malachite (SEM-EDS), mixite (μ Raman, EBSD)	Panel painting, Italy, 14th c
Smieska 2017 [34]	Azurite (SR-MAXRF; SR-MAXRD)	As, Ag, Ba, Bi, Fe, **Sb**, Zn, Zr (SR-XRF)	Calcite, hematite, malachite, barite (SR-MAXRD)	Manuscripts, Europe, 13–16th c
	Malachite	**Sb** (SR-MAXRF)	-	
Vanmeert 2018 [62]	Azurite	Fe, Ba (MAXRF)	Malachite, barite, quartz (?) (MAXRD)	Manuscript, not stated, 15/16th c
Vagnini 2018 [66]	Azurite, atacamite (XRD)	As, Fe, Cr, **Ni**, Mn, Ba/Ti (pXRF)	-	Wall painting, Italy, 13th c
Gabrieli 2019 [20]	Azurite (BR-RIS)	Zn, and Bi, As (pXRF)	Smithsonite ?, mixite (BR-RIS)	Manuscript, Italy, early Renaissance
Scrivano 2019 [63]	Azurite (μFTIR, μRaman)	Phosphates (P, Ce, Sm, Pr, La, Pb) (SEM-EDS)	Atacamite, paratacamite, malachite, mixite, carbon black (μRaman); monazite, pyromorphite, barite (SEM-EDS); silicates (μFTIR)	Marble fragments, Italy (Genoa), Middle Ages
Mastrotheodoros 2020 [68]	Azurite (EDS, μRaman)	As, Ba, Ca, Cl, Fe, **Ni**, **Sb**, Zn; Phosphates (P, La, Ce, Nd, Cu) (SEM-EDS/pXRF)	-	Icons, Greece, 15th–18th c
	Malachite (EDS, μRaman)	As, Ba, Ca, Mg, **Ni**, P, **Sb**, Zn (SEM-EDS/pXRF)	-	
Vetter 2021 [69]	Azurite (rFTIR, FORS)	Fe, Si (pXRF)	-	Manuscript, Italy, 13th c
Perino 2021 [70]	Azurite (FORS)	As, Bi, Zn (XRF)	-	Manuscripts, Italy, 14th c
Clarke 2021 [22]	Copper green (MAXRF)	As, Zn (MAXRF)	-	Handscroll, Japan, 13th c
Mazzinghi 2021 [71]	Azurite (MAXRF)	Zn, Ca (MAXRF)	-	Panel, Flanders, 15th c
Mihalic 2021 [72]	Azurite (PIXE+XRF)	Ba, Fe (PIXE+XRF)	-	Manuscript, Italy, 15th c
	Malachite (PIXE+XRF)	As, Ba, Fe, K, Mn, Pb, Si, Zn (PIXE+XRF)	-	

* Methods: SEM-EDS—scanning electron microscopy with energy-dispersive spectrometry; EBSD—Electron Backscatter Diffraction; (p)XRF—(portable) X-ray fluorescence; MAXRF—X-ray fluorescence mapping; SR—synchrotron radiation; XRD—X-ray powder diffraction; MAXRD—X-ray powder diffraction mapping; μFTIR—micro-Fourier transform infrared spectroscopy; rFTIR—external reflection Fourier transform infrared spectroscopy; BR-RIS—broad spectral range reflectance imaging spectroscopy; FORS—fiber optic reflectance spectroscopy; PIXE—particle induced X-ray emission; elements in bold—antimony and nickel impurities have been reported only rarely.

Antimony and nickel impurities have been reported only rarely (Table 5). In the case of the studied paint layers' samples (see Tables 1 and 2), antimony is almost always present in association with lead and, usually, arsenic. This is in accordance with the results of Mastrotheodoros et al. [68]. They reported, apart from Zn arsenates and barite, identification of antimony grains (Sb (Crete, 16th c), (unknown, 18th c); Sb-Pb (Crete 16th c); Sb-Zn-As, Sb-Cu-Pb (Crete, 17th c)) and grains containing nickel (Ni-Zn-As (Crete)) in azurite layers. In malachite layers, they reported finding, apart from Zn arsenates, barite, and dolomite, grains containing antimony (Zn-As-Sb-P (Ionian Islands, 17th c), Zn-As-Sb (Ionian Islands, 18th c)) and nickel (Zn-As-Ni (unknown, 18th c)). In Italian wall paintings, antimony and arsenic impurities were reported together with zinc [34], or barium [19]. In

our study, zinc was not detected in the paint layers but was present in the matrix in mineral specimens in the form of olivenite-adamite and conichalcite-austinite. Smieska et al. [34] correlated antimony and barium with azurite from a French manuscript. Nickel was also reported by Vagnini et al. [66] but interpreted as impurity of iron oxides. In this paper, we present impurities containing both elements, nickel and antimony together.

The presence or absence of impurities is used as an argument when determining the natural or artificial origin of the pigment [12]. The presence of some elements, such as zinc for brass [15] or tin for bronze, might be indicative of the artificial origin of copper pigments produced from metal alloys. Concurrent presence of copper, nickel, and tin, observed in the case of samples from the Ciechanowice Palace, may be linked with the use of bronze as the source of copper in the production of the artificial green copper pigment, verdigris, or a kind of calcium copper acetate, like in the recipes reported by Scott [2] and Krekel et al. [73]. In the blue-green paint layer, copper and calcium were detected as the main elements, while Raman spectroscopy detected calcite only, and copper pigment remained undetermined. Small inclusions of Pb-Sb-Cu-O, Cu-As-O, Cu-Sb-O, Sb-P-Cu-O, Sb-Pb-Cu-As-O, or Pb-As-Sb in bronze objects were described, which suggested that As-rich copper ores, such as copper sulphosalts of the tetrahedrite and tennatite series or copper arsenates could have been used as the source of copper [57]. In the case of Ciechanowice, the artificial origin of the copper pigment is likely, but to confirm it studies of reconstructions of old recipes for copper pigments would be needed.

Identification of accompanying phases in copper-bearing paint layers is often subject to theoretical speculations about the provenance of the pigment. Scrivano et al. [66] described two different mineralogical associations of azurite in the studied polychromy of marble fragments, and, based on historical data and accompanying phases (lead minerals, monazite), identified the Calabona mine in Sardinia as a possible provenance for one type of azurite. Nevertheless, these are ubiquitous phases with over 800 localities in Europe [54]; thus, the hypothesis needs to be confirmed by additional research. Hradil et al. [18] identified grains of malachite, olivenite, and, possibly, adamite in a sample of azurite, and, based on olivenite's presence in the deposit, pointed to Ľubietová as a possible provenance. However, olivenite is a common mineral phase, with 370 localities in Europe listed by mindat.org [54]. Based on historical data, the Slovakian origin of the pigment is probable, but in this case the chemical analyses cannot be regarded as conclusive evidence. Nevertheless, they may certainly be considered as one of the arguments to support the hypothesis about the Slovakian origin. Buzgar et al. [13] identified conichalcite and pointed to German provenance of the pigment and dolerophanite indicating Vesuvius sources. As shown in this study, conichalcite is ubiquitous (with more than 150 localities in Europe [54]), and it cannot be indicative of a specific region. The dolerophanite is indeed a rare mineral, thus it could be indicative of a particular type of deposit. Finding an impurity or a set of impurities of a copper pigment rare enough to be specific for a particular ore deposit or particular mine is a challenge. Moreover, not all historic mines have been studied, as they are often inaccessible. They were not of interest to the scientists if they had not had any economic significance. Thus, we do not have a good comparative database for provenance studies. As presented in this paper, a random study of minerals is not conclusive.

Therefore, it seems that, at the current state of knowledge, it is more appropriate to use impurities to group paintings than to trace the provenance of the pigment. Buzgar et al. [13] discerned two different workshops on the basis of conichalcite and dolerophanite presence. Smieska et al. [34] correlated azurite with silver and high concentration of barium with a Spanish manuscript, and iron, antimony, barium without zinc, arsenic, zirconium, and bismuth with a French manuscript. Švarcová et al. [12] classified the wall paintings of the Sázava monastery into groups. Berrie et al. [19] cited analyses of paintings attributed to Giotto, in which arsenic, antimony and barium were detected in areas painted with copper-based pigments, and herself identified a copper-bismuth arsenate, mixite, in an azurite layer exceptionally free from other impurities. It shows that specific impurities can be a helpful tool in establishing the artist's choice of color, and, in this respect, the authorship,

or simply in the studies of technical art history. It is important to remark that they provide hints not only about the source of the pigment, but also about the preparation, as all mineral pigments underwent purification. This should also be taken into consideration when grouping paintings.

In our study, the sample of copper pigment from Cracow Bishops' Palace in Kielce differs from the others as it contains bromine, aluminum and elevated concentrations of iron, and it does not contain tin nor nickel. Bromine has never been measured in the Miedzianka HMC deposit, but we cannot completely exclude its presence in low quantities. Among European localities with copper and bromine, Mindat.org lists the Ore Mountains in Czechia, Baden-Württemberg, Rhineland-Palatinate, and Saxony in Germany [54]. In this case, we may suggest with caution that the pigment was probably purchased from some more remote source than the local deposit. Our study showed some similarities between impurities of copper pigments in Ciechanowice and Chotków. In both places, tin was detected, and Cu-Ni-Sb phase was present (see G4/4, Ch35/1 in Table 2). Yet, there are also important differences between the two paintings, such as the type and morphology of the copper pigment. Furthermore, the concentrations of tin were much higher in samples from Ciechanowice Palace, most likely indicating the artificial origin of the pigment produced from bronze alloy.

Some of the above mentioned impurities might be overlooked during research, e.g., nickel in XRF analyses, due to the presence of impurities in the X-ray tube [71]. In EDS analysis, bromine might be misinterpreted because of possible overlap between the most characteristic X-ray peaks of Br and Al in low energies: Al Kα1 (1.487 keV)–Br Lα1 (1.480 keV). Lead is a common component of various pigments and is usually attributed to lead white, a pigment often mixed with copper pigments to achieve a lighter hue [36]. Nevertheless, cerussite and hydrocerussite are natural associates of malachite and azurite [54]. In sample K52, from the former Cracow Bishops' Palace in Kielce, lead areas are embedded inside the crystals of azurite (Figure 1), while in sample Ch35 (Figure 3), in a Cu-Ni-Sb crystal, which is clear evidence of an impurity. Antimony is often interpreted as an artificially produced pigment—Naples yellow (the equivalent of naturally occurring mineral—bindheimite). Still, it does not necessarily have to be correlated with lead, although most often is, as shown in our study. Our research proved that antimony might be accompanied by arsenic (antimony grains were found in olivenite/adamite and conichalcite matrix in mineral specimens), but also by nickel (in Cu-Ni-Sb grains in copper pigments), and tin and copper (Sn-Cu grains with variable content of Sb).

5. Conclusions

Analyses presented in this paper show how challenging it is to identify the accessory phase in a thin layer of paint. The problems encountered are mainly as follows: minute samples, small number of impurities, and low spatial resolution of laboratory devices. In this respect, macro-scanning methods, such as MAXRF or MAXRD would definitely be more efficient than point analyses. However, since they are more precise, point analyses of micro-samples, provide useful information for the interpretation of macro-scanning methods. As demonstrated above, impurities might be used to group paintings, define the artist choice of colors, determine whether the pigment was of natural or artificial origin, and, to some extent, support the hypothesis of the pigment's origin but, at the current state of the art, are usually not conclusive about its provenance. Comparison of results obtained from paint layers and from minerals helped to better understand the composition of the impurities and the matrix in which they might be embedded. Studies of minerals from the known sources have once again shown the risks researchers might face when provenance studies are based on the presence of more or less ubiquitous impurities.

References

1. Siddall, R. Mineral Pigments in Archaeology: Their Analysis and the Range of Available Materials. *Minerals* **2018**, *8*, 201. [CrossRef]
2. Scott, D.A.; Getty Conservation Institute. *Copper and Bronze in Art: Corrosion, Colorants, Conservation*; Getty Conservation Institute: Los Angeles, CA, USA, 2002.
3. Scott, D.A. A review of ancient Egyptian pigments and cosmetics. *Stud. Conserv.* **2016**, *61*, 185–202. [CrossRef]
4. Brecoulaki, H.; Fiorin, E.; Vigato, P.A. The funerary klinai of tomb 1 from Amphipolis and a sarcophagus from ancient Tragilos, eastern Macedonia: A physico-chemical investigation on the painting materials. *J. Cult. Herit.* **2006**, *7*, 301–311. [CrossRef]
5. Knipe, P.; Eremin, K.; Walton, M.; Babini, A.; Rayner, G. Materials and techniques of Islamic manuscripts. *Herit. Sci.* **2018**, *6*, 55. [CrossRef]
6. Tomasini, E.; Rodríguez, D.C.; Gómez, B.A.; de Faria, D.L.A.; Landa, C.R.; Siracusano, G.; Maier, M.S. A multi-analytical investigation of the materials and painting technique of a wall painting from the church of Copacabana de Andamarca (Bolivia). *Microchem. J.* **2016**, *128*, 172–180. [CrossRef]
7. Correia, A.M.; Clark, R.J.H.; Ribeiro, M.I.M.; Duarte, M.L.T.S. Pigment study by Raman microscopy of 23 paintings by the Portuguese artist Henrique Pousão (1859–1884). *J. Raman Spectrosc.* **2007**, *38*, 1390–1405. [CrossRef]
8. Daniel, F.; Mounier, A.; Aramendia, J.; Gómez, L.; Castro, K.; Fdez-Ortiz de Vallejuelo, S.; Schlicht, M. Raman and SEM-EDX analyses of the 'Royal Portal' of Bordeaux Cathedral for the virtual restitution of the statuary polychromy. *J. Raman Spectrosc.* **2016**, *47*, 162–167. [CrossRef]
9. Akyuz, T.; Akyuz, S.; Gulec, A. Elemental and spectroscopic characterization of plasters from Fatih Mosque-Istanbul (Turkey) by combined micro-Raman, FTIR and EDXRF techniques. *Spectrochim. Acta A Mol. Biomol. Spectrosc.* **2015**, *149*, 744–750. [CrossRef] [PubMed]
10. Spring, M. New insights into the materials of fifteenth- and sixteenth-century Netherlandish paintings in the National Gallery, London. *Herit. Sci.* **2017**, *5*. [CrossRef]
11. Naumova, M.M.; Pisareva, S.A. A note on the use of blue and green copper compounds in paintings. *Stud. Conserv.* **2013**, *39*, 277–283. [CrossRef]
12. Švarcová, S.; Hradil, D.; Hradilová, J.; Kočí, E.; Bezdicka, P. Micro-analytical evidence of origin and degradation of copper pigments found in Bohemian Gothic murals. *Anal. Bioanal. Chem.* **2009**, *395*, 2037–2050. [CrossRef]
13. Buzgar, N.; Buzatu, A.; Apopei, A.-I.; Cotiugă, V. In situ Raman spectroscopy at the Voroneţ Monastery (16th century, Romania): New results for green and blue pigments. *Vib. Spectrosc.* **2014**, *72*, 142–148. [CrossRef]
14. Aceto, M.; Gatti, G.; Agostino, A.; Fenoglio, G.; Giordano, V.; Varetto, M.; Castagneri, G. The mural paintings of Ala di Stura (Piedmont, Italy): A hidden treasure investigated. *J. Raman Spectrosc.* **2012**, *43*, 1754–1760. [CrossRef]
15. Alejandre, F.J.; Márquez, G. Copper-zinc hydroxychlorides: Origin and occurrence as paint pigments in Arcos de la Frontera's Chapel of Mercy (Spain). *Eur. J. Mineral.* **2006**, *18*, 403–409. [CrossRef]
16. Available online: https://rruff.info/ima/ (accessed on 25 October 2021).
17. Garcia Moreno, R.; Strivay, D.; Gilbert, B. Maya blue-green pigments found in Calakmul, Mexico: A study by Raman and UV-visible spectroscopy. *J. Raman Spectrosc.* **2008**, *39*, 1050–1056. [CrossRef]
18. Hradil, D.; Hradilová, J.; Bezdička, P.; Švarcová, S. Provenance study of Gothic paintings from North-East Slovakia by handheld x-ray fluorescence, microscopy and x-ray microdiffraction. *X-ray Spectrom.* **2008**, *37*, 376–382. [CrossRef]
19. Berrie, B.H.; Leona, M.; McLaughlin, R. Unusual pigments found in a painting by Giotto (c. 1266-1337) reveal diversity of materials used by medieval artists. *Herit. Sci.* **2016**, *4*. [CrossRef]

20. Gabrieli, F.; Dooley, K.A.; Facini, M.; Delaney, J.K. Near-UV to mid-IR reflectance imaging spectroscopy of paintings on the macroscale. *Sci. Adv.* **2019**, *5*, eaaw7794. [CrossRef]

21. Klisińska-Kopacz, A. Non-destructive characterization of 17th century painted silk banner by the combined use of Raman and XRF portable systems. *J. Raman Spectrosc.* **2015**, *46*, 317–321. [CrossRef]

22. Clarke, M.L.; Gabrieli, F.; Rowberg, K.L.; Hare, A.; Ueda, J.; McCarthy, B.; Delaney, J.K. Imaging spectroscopies to characterize a 13th century Japanese handscroll, The Miraculous Interventions of Jizō Bosatsu. *Herit. Sci.* **2021**, *9*, 20. [CrossRef]

23. Dunkerton, J.; Roy, A. The Materials of a Group of Late Fifteenth-century Florentine Panel Paintings. *Natl. Gallery Tech. Bull.* **1996**, *17*, 20–31.

24. Zaffino, C.; Guglielmi, V.; Faraone, S.; Vinaccia, A.; Bruni, S. Exploiting external reflection FTIR spectroscopy for the in-situ identification of pigments and binders in illuminated manuscripts. Brochantite and posnjakite as a case study. *Spectrochim. Acta A Mol. Biomol. Spectrosc.* **2015**, *136 Pt B*, 1076–1085. [CrossRef]

25. Mugnaini, S.; Bagnoli, A.; Bensi, P.; Droghini, F.; Scala, A.; Guasparri, G. Thirteenth century wall paintings under the Siena Cathedral (Italy). Mineralogical and petrographic study of materials, painting techniques and state of conservation. *J. Cult. Herit.* **2006**, *7*, 171–185. [CrossRef]

26. Sotiropoulou, S.; Daniilia, S.; Miliani, C.; Rosi, F.; Cartechini, L.; Papanikola-Bakirtzis, D. Microanalytical investigation of degradation issues in Byzantine wall paintings. *Appl. Phys. A* **2008**, *92*, 143–150. [CrossRef]

27. Rosado, T.; Gil, M.; Caldeira, A.T.; Martins, M.d.R.; Dias, C.B.; Carvalho, L.; Mirão, J.; Candeias, A.E. Material Characterization and Biodegradation Assessment of Mural Paintings: Renaissance Frescoes from Santo Aleixo Church, Southern Portugal. *Int. J. Archit. Herit.* **2014**, *8*, 835–852. [CrossRef]

28. Švarcová, S.; Hradil, D.; Hradilová, J.; Čermáková, Z. Pigments—Copper-based greens and blues. *Archaeol. Anthropol. Sci.* **2021**, *13*, 190. [CrossRef]

29. Tanevska, V.; Nastova, I.; Minčeva-Šukarova, B.; Grupče, O.; Ozcatal, M.; Kavčić, M.; Jakovlevska-Spirovska, Z. Spectroscopic analysis of pigments and inks in manuscripts: II. Islamic illuminated manuscripts (16th–18th century). *Vib. Spectrosc.* **2014**, *73*, 127–137. [CrossRef]

30. Perez-Alonso, M.; Castro, K.; Madariaga, J.M. Investigation of degradation mechanisms by portable Raman spectroscopy and thermodynamic speciation: The wall painting of Santa Maria de Lemoniz (Basque Country, North of Spain). *Anal. Chim Acta* **2006**, *571*, 121–128. [CrossRef] [PubMed]

31. Bersani, D.; Antonioli, G.; Lottici, P.P.; Casoli, A. Raman microspectrometric investigation of wall paintings in S. Giovanni Evangelista Abbey in Parma: A comparison between two artists of the 16th century. *Spectrochim. Acta A Mol. Biomol. Spectrosc.* **2003**, *59*, 2409–2417. [CrossRef]

32. Valadas, S.; Freire, R.V.; Cardoso, A.; Mirão, J.; Dias, C.B.; Vandenabeele, P.; Candeias, A. On the Use of the Unusual Green Pigment Brochantite ($Cu_4(SO_4)(OH)_6$) in the 16th-Century Portuguese-Flemish Paintings Attributed to The Master Frei Carlos Workshop. *Microsc. Microanal.* **2015**, *21*, 518–525. [CrossRef] [PubMed]

33. Aru, M.; Burgio, L.; Rumsey, M.S. Mineral impurities in azurite pigments: Artistic or natural selection? *J. Raman Spectrosc.* **2014**, *45*, 1013–1018. [CrossRef]

34. Smieska, L.M.; Mullett, R.; Ferri, L.; Woll, A.R. Trace elements in natural azurite pigments found in illuminated manuscript leaves investigated by synchrotron x-ray fluorescence and diffraction mapping. *Appl. Phys. A* **2017**, *123*. [CrossRef]

35. Delaney, J.K.; Ricciardi, P.; Glinsman, L.D.; Facini, M.; Thoury, M.; Palmer, M.; Rie, E.R.d.l. Use of imaging spectroscopy, fiber optic reflectance spectroscopy, and X-ray fluorescence to map and identify pigments in illuminated manuscripts. *Stud. Conserv.* **2014**, *59*, 91–101. [CrossRef]

36. Salvadó, N.; Butí, S.; Aranda, M.A.G.; Pradell, T. New insights on blue pigments used in 15th century paintings by synchrotron radiation-based micro-FTIR and XRD. *Anal. Methods* **2014**, *6*. [CrossRef]

37. Siuda, R.; Domańska-Siuda, J. STOP 1: Miedzianka deposit—one of the oldest mining centres in Poland. In Proceedings of the XXVIth Meeting of the Petrology Group of the Mineralogical Society of Poland, Chęciny, Poland, 24–27 October 2019; pp. 99–103.

38. Siuda, R.; Borzęcki, R.; Gołębiowska, B. Hałdy dawnego górnictwa w rejonie Miedzianki-Ciechanowic jako stanowiska dokumentacyjne unikatowej mineralizacji hipergenicznej. In Proceedings of the Dzieje Górnictwa—Element Europejskiego Dziedzictwa Kultury, Wrocław, Poland, 3 January 2010; pp. 431–441.

39. Witkowski, M.; Svorová Pawełkowicz, S. Handel pigmentami miedziowymi ze złóż świętokrzyskich w świetle źródeł archiwalnych. *AUNC Zabytkozn. I Konserw.* **2021**, forthcoming.

40. Hauptmann, A.; Schneider, G.; Bartels, C. The Shipwreck of "Bom Jesus", AD 1533: Fugger Copper in Namibia. *J. Afr. Archaeol.* **2016**, *14*, 181–207. [CrossRef]

41. Dzik, J. The Famennian "Golden Age" of Conodonts and Ammonoids in the Polish Part of the Variscan Sea. *Palaeontol. Pol.* **2006**, *63*, 1–360.

42. Rubinowski, Z. Rudy metali nieżelaznych w Górach Świętokrzyskich i ich pozycja metalogeniczna. *Biul. Inst. Geol.* **1971**, *247*, 1–166.

43. Rubinowski, Z. Nowe obserwacje okruszcowania na Miedziance świętokrzyskiej. *Przegląd Geol.* **1955**, *6*, 299–301.

44. Mazur, S.; Aleksandrowski, P. The Tepla(?)/Saxothuringian suture in the Karkonosze–Izera massif, western Sudetes, central European Variscides. *Int. J. Earth Sci.* **2001**, *90*, 341–360. [CrossRef]

45. Mikulski, S.Z.; Williams, I.S.; Stein, H.J.; Wierchowiec, J. Zircon U-Pb Dating of Magmatism and Mineralizing Hydrothermal Activity in the Variscan Karkonosze Massif and Its Eastern Metamorphic Cover (SW Poland). *Minerals* **2020**, *10*, 787. [CrossRef]

46. Parafiniuk, J.; Siuda, R.; Borkowski, A. Sulphate and arsenate minerals as environmental indicators in the weathering zones of selected ore deposits, Western Sudetes, Poland. *Acta Geol. Pol.* **2016**, *66*, 493–508. [CrossRef]

47. Vozarova, A.; Konečný, P.; Vďačný, M.; Vozár, J.; Šarinová, K. Provenance of Permian Malužiná Formation sandstones (Hronicum, Western Carpathians): Evidence from monazite geochronology. *Geol. Carpathica* **2014**, *65*, 329–338. [CrossRef]

48. Michňová, J.; Ozdín, D. Genetic study of the primary hydrothermal mineralization in Špania Dolina and Ľubietová ore districts (Slovakia, Western Carpathians). *Acta Mineral. Petrogr.* **2010**, *6*, 237.

49. Radkova Borcinova, A.; Jamieson, H.; Lalinská-Voleková, B.; Majzlan, J.; Števko, M.; Chovan, M. Mineralogical controls on antimony and arsenic mobility during tetrahedrite-tennantite weathering at historic mine sites Špania Dolina-Piesky and Ľubietová-Svätodušná, Slovakia. *Am. Mineral.* **2017**, *102*, 1091–1100. [CrossRef]

50. Coccato, A.; Moens, L.; Vandenabeele, P. On the stability of mediaeval inorganic pigments: A literature review of the effect of climate, material selection, biological activity, analysis and conservation treatments. *Herit. Sci.* **2017**, *5*, 12. [CrossRef]

51. Švarcová, S.; Čermáková, Z.; Hradilová, J.; Bezdička, P.; Hradil, D. Non-destructive micro-analytical differentiation of copper pigments in paint layers of works of art using laboratory-based techniques. *Spectrochim. Acta Part. A Mol. Biomol. Spectrosc.* **2014**, *132*, 514–525. [CrossRef]

52. Mattei, E.; de Vivo, G.; De Santis, A.; Gaetani, C.; Pelosi, C.; Santamaria, U. Raman spectroscopic analysis of azurite blackening. *J. Raman Spectrosc.* **2008**, *39*, 302–306. [CrossRef]

53. Castro, K.; Sarmiento, A.; Martínez-Arkarazo, I.; Madariaga, J.M.; Fernández, L.A. Green Copper Pigments Biodegradation in Cultural Heritage: From Malachite to Moolooite, Thermodynamic Modeling, X-ray Fluorescence, and Raman Evidence. *Anal. Chem.* **2008**, *80*, 4103–4110. [CrossRef]

54. Available online: www.mindat.org (accessed on 13 September 2021).

55. Stavinga, D.; Jamieson, H.; Layton-Matthews, D.; Paradis, S.; Falck, H. Geochemical and mineralogical controls on metal(loid) mobility in the oxide zone of the Prairie Creek Deposit, NWT. *Geochem. Explor. Environ. Anal.* **2017**, *17*, 21–33. [CrossRef]

56. Kühn, H. 4 LEAD-TIN YELLOW. *Stud. Conserv.* **1968**, *13*, 7–33. [CrossRef]

57. Bugaj, U.; Nejbert, K.; Ilnicki, S.; Wiecinski, P.; Onyszczuk, T.; Halina, G.; Włodarczak, P. Copper sulphosalts in early metallurgy (2600–1900 BC)—Chemical-mineralogical investigation of artefacts from southern Poland. *Geol. Q.* **2019**, *63*. [CrossRef]

58. Frost, R.L.; Martens, W.N.; Williams, P.A. Raman spectroscopy of the phase-related basic copper arsenate minerals olivenite, cornwallite, cornubite and clinoclase. *J. Raman Spectrosc.* **2002**, *33*, 475–484. [CrossRef]

59. Swęd, M.; Urbanek, P.; Krechowicz, I.; Dworczak, P.; Wiecka, P.; Mleczak, M.; Tobys, P. Mineralogia hałd wietrzeniowych złoża Miedzianka (Góry Świętokrzyskie). *Przegląd Geol.* **2015**, *63*, 363–372.

60. Gałuszka, A.; Migaszewski, Z.M.; Dołęgowska, S.; Michalik, A.; Duczmal-Czernikiewicz, A. Geochemical background of potentially toxic trace elements in soils of the historic copper mining area: A case study from Miedzianka Mt., Holy Cross Mountains, south-central Poland. *Env. Earth Sci.* **2015**, *74*, 4589–4605. [CrossRef]

61. Burgio, L.; Clark, R.J.H.; Hark, R.R. Raman microscopy and X-ray fluorescence analysis of pigments on medieval and Renaissance Italian manuscript cuttings. *Proc. Natl. Acad. Sci. USA* **2010**, *107*, 5726–5731. [CrossRef]

62. Vanmeert, F.; De Nolf, W.; De Meyer, S.; Dik, J.; Janssens, K. Macroscopic X-ray Powder Diffraction Scanning, a New Method for Highly Selective Chemical Imaging of Works of Art: Instrument Optimization. *Anal. Chem.* **2018**, *90*, 6436–6444. [CrossRef]

63. Scrivano, S.; Gaggero, L.; Volpe, E. Paint Relics on Middle Age Building Stones as Proxies of Commercial Routes and Artistic Exchanges: A Multi-Analytical Investigation. *Minerals* **2019**, *9*, 663. [CrossRef]

64. Bordignon, F.; Postorino, P.; Dore, P.; Tabasso, M.L. The Formation of Metal Oxalates in the Painted Layers of a Medieval Polychrome on Stone, as Revealed by Micro-Raman Spectroscopy. *Stud. Conserv.* **2008**, *53*, 158–169. [CrossRef]

65. Fabjan, B.; Dalla Nave, P.; Moioli, P.; Seccorani, C.; Cardinali, M.; De Ruggieri, M.B.; Falucci, C. La volta del coro di Santa Maria del Popolo a Roma. In Proceedings of the Materiali e Tecniche Nella Pittura Murale Del Quattrocento, Rome, Italy, 20–22 February 2002; pp. 437–452.

66. Vagnini, M.; Vivani, R.; Viscuso, E.; Favazza, M.; Brunetti, B.G.; Sgamellotti, A.; Miliani, C. Investigation on the process of lead white blackening by Raman spectroscopy, XRD and other methods: Study of Cimabue's paintings in Assisi. *Vib. Spectrosc.* **2018**, *98*, 41–49. [CrossRef]

67. Aceto, M.; Agostino, A.; Fenoglio, G.; Capra, V.; Demaria, E.; Cancian, P. Characterisation of the different hands in the composition of a 14th century breviary by means of portable XRF analysis and complementary techniques: Different hands in a 14th-century breviary by means of XRF analysis. *X-ray Spectrom.* **2017**, *46*. [CrossRef]

68. Mastrotheodoros, G.P.; Beltsios, K.G.; Bassiakos, Y. On the blue and green pigments of post-Byzantine Greek icons. *Archaeometry* **2020**, *62*, 774–795. [CrossRef]

69. Lannoy, A.; Kania, N.; Bleta, R.; Fourmentin, S.; Machut-Binkowski, C.; Monflier, E.; Ponchel, A. Photocatalysis of Volatile Organic Compounds in water: Towards a deeper understanding of the role of cyclodextrins in the photodegradation of toluene over titanium dioxide. *J. Colloid Interface Sci.* **2016**, *461*, 317–325. [CrossRef] [PubMed]

70. Perino, M.; Pronti, L.; Di Forti, L.G.; Romani, M.; Taverna, C.; Massolo, L.; Manzari, F.; Cestelli-Guidi, M.; Nucara, A.; Felici, A.C. Revealing Artists' Collaboration in a 14th Century Manuscript by Non-Invasive Analyses. *Minerals* **2021**, *11*, 771. [CrossRef]

71. Mazzinghi, A.; Ruberto, C.; Castelli, L.; Czelusniak, C.; Giuntini, L.; Mando, P.A.; Taccetti, F. MA-XRF for the Characterisation of the Painting Materials and Technique of the Entombment of Christ by Rogier van der Weyden. *Appl. Sci.* **2021**, *11*, 6151. [CrossRef]
72. Mihalic, I.B.; Fazinic, S.; Barac, M.; Karydas, A.G.; Migliori, A.; Doracic, D.; Desnica, V.; Mudronja, D.; Krstic, D. Multivariate analysis of PIXE plus XRF and PIXE spectral images. *J. Anal. At. Spectrom.* **2021**, *36*, 654–667. [CrossRef]
73. Krekel, C.; Polborn, K. Lime Blue—A Mediaeval Pigment for Wall Paintings? *Stud. Conserv.* **2003**, *48*, 171–182. [CrossRef]